Atmos. Meas. Tech., 9, 1083–1094, 2016
www.atmos-meas-tech.net/9/1083/2016/
doi:10.5194/amt-9-1083-2016

Atmospheric Measurement Techniques
Open Access
EGU

Calibration of a water vapour Raman lidar with a kite-based humidity sensor

Julien Totems and Patrick Chazette

Laboratoire des Sciences du Climat et de l'Environnement, CEA, Gif-sur-Yvette, France

Correspondence to: Julien Totems (julien.totems@lsce.ipsl.fr)

Received: 6 August 2015 – Published in Atmos. Meas. Tech. Discuss.: 15 October 2015
Revised: 3 February 2016 – Accepted: 24 February 2016 – Published: 15 March 2016

Abstract. We present a calibration method for a water vapour Raman lidar using a meteorological probe lifted by a kite, flown steadily above the lidar site, within the framework of the Hydrological Cycle in the Mediterranean Experiment (HyMeX) and Chemistry-Aerosol Mediterranean Experiment (ChArMEx) campaigns. The experiment was carried out in Menorca (Spain) during June 2013, using the mobile water vapour and aerosol lidar WALI. Calibration using a kite demonstrated a much better degree of co-location with the lidar system than that which could be achieved with radiosondes, and it allowed us to determine the overlap function and calibration factor simultaneously. The range-dependent water vapour lidar calibration was thus determined with an uncertainty of 2 % in the 90–8000 m altitude range. Lidar water vapour measurements are further compared with radiosondes, showing very good agreement in the lower troposphere (1–5 km) and a relative difference and standard deviation of 5 and 9 % respectively. Moreover, a reasonable agreement with MODIS-integrated water vapour content is found, with a relative mean and standard deviation of 3 and 16 % respectively. However, a discrepancy is found with AERONET retrievals, showing the latter to be underestimated by 28 %. Reanalyses by the ECMWF/IFS numerical weather prediction model also agree with the temporal evolution highlighted with the lidar, with no measurable drift in integrated water vapour content over the period.

1 Introduction

Because of its role in the energy balance of the atmosphere, water vapour content is an essential parameter that drives atmospheric dynamics in and above the planetary boundary layer (PBL), as well as the hydrological cycle and of course cloud formation (Kulmala, 1993; Melfi et al., 1989). Due to the hygroscopic properties of airborne particles (e.g. Rood et al., 1987; Randriamiarisoa et al., 2006), it also acts on the radiative balance at a global scale (Haywood et al., 1997) by enhancing the extinction power of plumes containing hydrophilic aerosols. This is one of the reasons why aerosols remain a major source of uncertainty in long-term forecasts of radiative forcing on the climate (IPCC, 2014). For the past 3 years, within the French MISTRALS (Mediterranean Integrated Studies at RegionAL Scales) research program, the western Mediterranean basin has been the focus of both water cycle (Hydrological Cycle in the Mediterranean Experiment (HyMeX); Drobinski et al., 2014) and aerosol radiative forcing studies (Chemistry-Aerosol Mediterranean Experiment (ChArMEx); Mallet et al., 2015) because of the important societal impact of climate change in this densely populated region as well as its complex atmospheric circulation which makes both weather and chemical transport models fail to deliver reliable forecasts.

In this context, the range-resolved profiles of aerosol extinction and water vapour mixing ratio (WVMR) obtained by lidar remote sensing are a powerful tool. Raman lidars can measure WVMR through the calibrated ratio of water vapour and nitrogen inelastic backscatter signals (Whiteman et al., 1992). During the International H_2O Project IHOP (Weckwerth et al., 2004) in the American Great Plains, a radiosonde-calibrated system (Whiteman et al., 2006a) enabled the first study of water-vapour-driven convective processes in the PBL through the diurnal cycle (Whiteman et al., 2006b). The European Convective Orographic Precipitation Study COPS (Wulfmeyer et al., 2011) undertaken in 2007 in the Rhine Valley showed among other findings that

biases between several Raman and DIAL (DIfferential Absorption Lidar) water vapour lidars and passive remote sensing measurements remained below 5 % (Bhawar et al., 2011). Such systems still operational in Europe include the Raman lidars of BASIL (Di Girolamo and Summa, 2009) and IGN (Bock et al., 2013) institutes, the upper tropospheric/lower stratospheric Raman lidars at the Haute-Provence (Sherlock et al., 1999a) and Réunion (Dionisi et al., 2015) observatories and the scanning DIAL of the University of Hohenheim (Behrendt et al., 2009).

The water vapour and aerosol lidar WALI (Chazette et al., 2014a) is a portable and versatile system originally designed to meet the scientific goals of the first special observation period of HyMeX (Ducrocq et al., 2014) in autumn 2012. HyMeX is dedicated to the study of the water cycle and the role of water vapour and aerosols in cloud formation, leading specifically to the intense precipitation in the western basin during the autumn season, using multiple instruments in synergy and coupling their measurements to mesoscale models. Its overarching goal is to improve forecasts of extreme precipitation events on the orography of the western basin. WALI was also implemented as part of the Menorca Island (Spain) Cap d'en Font ground-based station during the June 2013 special observation period of the ADRIMED (Aerosol Direct Radiative Impact of the regional climate in the Mediterranean region; Mallet et al., 2015) segment of ChArMEx. ChArMEx aims to assess the present and future state of the atmosphere (gaseous reactive species and aerosol particles) in the Mediterranean basin, while its ADRIMED segment focuses on how the Mediterranean climate is impacted by direct aerosol forcing and may evolve in the next 50 years due to climate change and growing anthropic pressure. It involved ground and airborne instruments to study among others water vapour and aerosol coupling during summertime dust and pollution events in the western basin.

The proper absolute calibration of the WVMR derived by a Raman lidar, with less than $0.4\,\mathrm{g\,kg^{-1}}$ total uncertainty as demanded by meteorological and climate applications (NCAR/NOAA; Weckwerth et al., 1999), remains a critical issue. Indeed, several studies have shown that a purely photometric calibration performed on a laboratory optical bench to determine the gain ratio of the H_2O and N_2 paths lacks precision and leads to significant bias on the retrieved WVMR (a few $\mathrm{g\,kg^{-1}}$, $\sim 10\,\%$ in the lower troposphere; Leblanc and McDermid, 2008; Whiteman et al., 2011). This calibration method also requires a common optical path before the field diaphragm of the lidar, which was dismissed for WALI in favour of modularity. A more precise yet practical approach using the sky background as a standard light source (Sherlock et al., 1999b) requires radiative transfer models and elimination of all parasitic light sources. This was impossible in the set-up of this field experiment, where an anti-dust blowing funnel was necessary above the lidar windows, which scattered some sunlight onto the receptor. Raman lidars can also be calibrated using water vapour profiles given by a multi-channel microwave radiometer, as was done recently in the framework of the HD(CP)2 campaign in Germany, in an automated fashion (Foth et al., 2015). However, this instrument is still unavailable commercially. In the end, co-located vertical sounding to deduce WVMR from temperature and relative humidity (RH) measurements up to the stratosphere is the most precise method available, albeit limited by the accuracy of the meteorological probe. Radiosoundings are, however, rather heavy, with costly apparatus and a flight exclusion area needed to be granted by air traffic control. Moreover, they may drift and not always be well co-located with the lidar. Whereas the spatial homogeneity of WVMR is generally good in the free troposphere, it is less so in the PBL, especially in a coastal area or close to orography.

Incidentally, there is a long history of kite atmospheric sounding, which started with the "meteorographs" of Teisserenc de Bort at Trappes, France, in 1898. Despite an impressive altitude range (up to 9800 m in 1916), this technique was lost during the 20th century in favour of weather balloons. Due to the specific advantages of kites the team of Balsley et al. (1992, 1998) at CIRES reinstated their use and improved the technique for profiling the atmosphere. Indeed, materials and fabrics have evolved making kites lighter, less expensive and easier to handle. They also offer the possibility of sounding the same layer for a longer time and remaining stationary, like tethered balloons. They have been applied to low-altitude water vapour sounding (Davidson et al., 2003) or used for aerosol profiling (Reiche et al., 2012). Willitsford and Philbrick (2005) used the data of Davidson et al. (2003) in synergy with a ground-based Raman lidar to describe the evaporation duct over the ocean. Generally, the use of kites is only limited by adverse wind conditions and strict local regulations due to ever-increasing air traffic.

In this article, we present an original calibration process of a mobile water vapour Raman lidar using a kite-borne Vaisala pressure/temperature/RH probe, flying at low altitude where the lidar signal is strongest and biases due to temperature and aerosols transmission remain limited. This calibration is validated by comparisons to balloon profiling, remote sensing of integrated water content, and outputs from a meteorological model.

In Sect. 2 we will describe the set-up of the kite payload and WALI lidar, along with the location of the experiment and the exogenous measurements used in this study. Section 3 will present the calibration method and the assessment of the associated uncertainties. The cross-validation is presented in Sect. 4, where the lidar-derived WVMR profile and integrated water vapour content are compared with radiosoundings, satellite measurements (Moderate-resolution Imaging Spectroradiometer, MODIS), ground-based sun photometer measurements and reanalyses by the numerical weather prediction model ECMWF/IFS (European Centre for Medium-range Weather Forecasts/integrated forecast system). Section 5 will summarise and conclude.

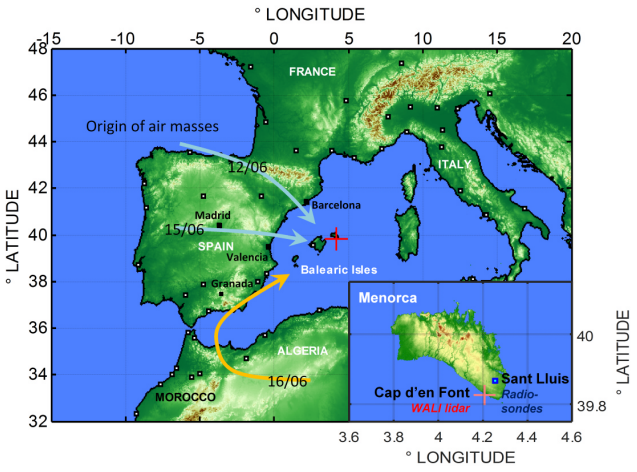

Figure 1. Situation map of the Menorca/Cap d'en Font station (red cross). The launch site of radiosoundings on Menorca island is shown as a blue square within the insert. Origins of air masses on the dates of lidar/radiosonde intercomparisons are noted as coloured arrows (Menorca digital elevation model courtesy of NASA/ASTER GDEM).

2 Experimental set-up

2.1 Location of the experiment

During the ADRIMED SOP-1 campaign in June to July 2013, a background station was deployed near the centre of the western Mediterranean, at Cap d'en Font (39°49′33″ N, 4°12′29″ E), a cape on the southern coast of the island of Menorca (Fig. 1). This site was chosen to stay clear of local pollution sources in the dominant south-westerly winds. It provides the opportunity to sample various air masses with contrasted water vapour amounts within the lower and middle troposphere. Moreover, the windy southern coast of Menorca is a very suitable environment to use a light instrumented kite.

2.2 Raman lidar WALI

The WALI is a transportable lidar instrument mainly dedicated to atmospheric research activities (Chazette et al., 2014a, b, 2015a). Emitting at a wavelength of 354.7 nm, it is designed to fulfil eye safety conditions. Its emitter is a pulsed Nd:YAG (Quantel Brilliant) laser. The UV pulse energy is ~ 60 mJ and the pulse repetition frequency is 20 Hz. Its wide field of view of ~ 2.3 mrad ensures a full overlap of the transmitter and receiver paths beyond ~ 200–300 m.

The system has three receivers and a total of four channels. On each channel, optical detection is performed by a photomultiplier tube (PMT) placed behind interferential filters (0.2 nm bandwidth) manufactured by Materion/Barr and a focusing lens. The amplification gain of the PMT between its anode and cathode is directly linked to the input high voltage (HV) chosen by the lidar acquisition software. Automatic HV variation allows optimisation of the detection dynamic range for both night-time and daytime measurements (with strong sky background light). In the following, gain variation is corrected after calibration of gain versus HV as in Chazette et al. (2014a), and water vapour calibration is given for fixed night-time values of HVs. The acquisition system is based on PXI technology with 12 bit digitisers running at 200 MS s^{-1} (mega sampling per second), manufactured by National Instruments. Throughout the experiment acquisition was performed for mean profiles of 1000 laser shots, leading to a temporal sampling close to 1 min.

The first receiver, with two channels (co- and cross-polarised), is dedicated to the detection of the elastic molecular, aerosols and cloud backscatter from the atmosphere. The second and third receivers are dedicated to the measurements of the inelastic nitrogen (N_2 channel, ~ 387 nm) and water vapour (H_2O channel, ~ 407 nm) Raman backscattered signals respectively. They are identical to the elastic receiver except for interference filters centred at the respective wavelengths of the first Stokes vibrational lines for the two gases (386.65 ± 0.10 and 407.45 ± 0.15 nm filter bandpass respectively) and an extra dichroic beam splitter on the H_2O channel for better rejection of the elastic returns (complete details are given in Chazette et al., 2014a).

The WVMR is obtained as the ratio between the signals recorded by the H_2O and N_2 Raman channels. In previous experiments with a properly calibrated WALI (Chazette et al., 2014a), the uncertainty on the WVMR reached 11 % in the marine boundary layer and decreased to 7 % below the 5 km range, with temporal averaging over 20 min and a nominal vertical resolution of 15 m. Precision deteriorated quickly above 5 km above mean sea level (a.m.s.l.) due to the decreasing signal-to-noise ratio (SNR), which we compensate here with larger averaging. The determination of the water vapour profile is more difficult during daytime due to low SNR, but the measurements have been performed with sufficient precision for altitude ranges below ~ 1 km a.m.s.l. using temporal averaging over ~ 30 min. A low-altitude WVMR calibration directly above the lidar is especially interesting considering that the progressive overlap of the lidar emission and reception paths biases WVMR up to 300 m, as noticed in the previous deployment of the lidar.

2.3 Water vapour sounding

Kites were launched directly from Cap d'en Font, 100 m from the lidar. The apparatus used for kite sounding is shown on Fig. 2. The kites were both "rokkaku" (hexagonal) kites (1.3 or 1.5 m width, for winds 3–15 m s^{-1}, with vented sails for improved stability) at the end of a single 650 m braided polyester line, carrying a lightweight (360 g) probe and data logger (Vaisala PTB-110 barometer + Vaisala SP 2000-35R T/RH/V datalogger $+2 \times 9$ V batteries). This length of line

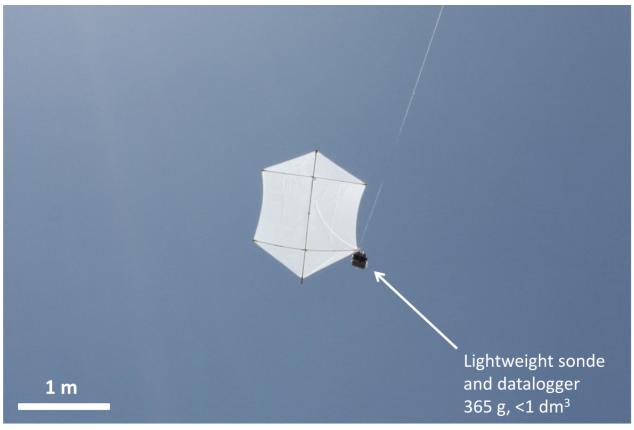

Figure 2. View of the rokkaku kite and lightweight sonde and data logger assembly used for lidar calibration.

allowed for an approximate maximum sounding altitude of 450 m given the payload and wind conditions encountered in Menorca. Data were recorded every 10 s and retrieved after the flight. Given the specifications in Table 1, the expected absolute accuracy on each WVMR sample is 0.6 g kg^{-1}.

A CNES team led by N. Verdier launched radiosondes on weather balloons, along with particle and ozone counters, at the Sant-Lluís air field (39°51′56″ N, 4°15′17″ E), located 8 km northeast of the WALI lidar at Cap d'en Font. This airfield was the only site where radiosounding could be organised, authorised and made compatible with air traffic to and from the nearby Mahon airport, whereas the aerosol/lidar station had to stay on the coast. The characteristics of the Modem M10 GPSondes used are also given in Table 1. From these data, an absolute uncertainty of 1.2 g kg^{-1} is expected near the ground (mostly due to the inaccuracy of the GPS altitude), which goes down to 0.04 g kg^{-1} at 10 km a.m.s.l.

At ground level, a Vaisala PTU-300, set on a 6 m mast protruding from the mobile laboratory where WALI was embedded, yielded WVMR measurements with an accuracy of 0.3 g kg^{-1}.

The Cap d'en Font station was also equipped with a Cimel sun photometer as part of the Aerosol RObotic NETwork (AERONET, http://http://aeronet.gsfc.nasa.gov/) for the duration of the campaign. It provided regular measurements of precipitable water vapour in the atmospheric column, simultaneously with aerosol optical thickness and Angström exponent.

2.4 Spaceborne measurements and numerical weather prediction model

On board the Aqua and Terra satellite, launched in the early 2000s as part of the Earth Observing System, MODIS captures images in 36 spectral bands to provide measurements of large-scale global dynamics, including in the lower atmosphere. MODIS level 3 data sets are available online from NASA (https://earthdata.nasa.gov/labs/worldview/). They include daily precipitable water vapour data given on a 1° grid on both land and sea, with sufficient accuracy to allow comparison with ground-based measurements of water vapour (Gao and Kaufman, 2003).

Table 1. Characteristics of the WVMR in situ sounding apparatus.

Kite PTU sonde (LSCE), Vaisala modules and recorder (360g)	
Altitude range	5–400 m
Measurements	Temperature, RH, pressure
Meas. period	10 s
Temp. uncertainty	±0.15 °C
RH uncertainty	±2 %
Pressure uncertainty	±0.6 hPa
→ WVMR error	±0.6 g kg^{-1} (below 500 m)
Balloon rawinsounding (CNES), Modem GPSonde M10 (150g)	
Altitude range	100 m–36 km a.m.s.l.
Measurements	Temperature, RH, GPS altitude
Meas. period	1 s
Temp. uncertainty	±0.5 °C
RH uncertainty	±5 %
Altitude uncertainty	±10 m (±1 hPa down to 0.4 hPa at 10 km a.m.s.l.)
→ WVMR error	±1.2 g kg^{-1} down to ±0.04 g kg^{-1} at 10 km a.m.s.l.

Modelled synoptic-scale meteorological fields (geopotential height, temperature, moisture) have been obtained over a large domain around the western Mediterranean from the IFS of the ECMWF (http://www.ecmwf.int). The 3-D fields, available on the ESPRI/IPSL data server, are 6-hourly reanalyses with a horizontal resolution of 0.5°. The ECMWF model produces a good representation of the low-resolution moisture field as demonstrated in previous works (Chazette et al., 2014b).

3 Lidar calibration

With the WALI lidar, the WVMR profile is obtained as

$$r_{\mathrm{H_2O,lidar}}(z) = K_{\mathrm{WVMR}} \frac{S_{\mathrm{H_2O}}(z)/\xi_{\mathrm{H_2O}}(z)}{S_{\mathrm{N_2}}(z)/\xi_{\mathrm{N_2}}(z)} \exp(\Delta\tau(z)), \quad (1)$$

where K_{WVMR} is a constant to be calibrated, $S_{\mathrm{H_2O}}(z)$ and $S_{\mathrm{N_2}}(z)$ are the lidar signals in the indexed channels, expressed as a function of altitude z, and $\xi_{\mathrm{H_2O}}(z)$ and $\xi_{\mathrm{N_2}}(z)$ are the lidar overlap factors of the indexed channels (both reach 1 above 400 m). Correction factor $\Delta\tau(z)$ is the difference of total optical thickness between wavelengths 387 and 407 nm, which has to be estimated from the aerosol channel and the Angström exponent of the aerosols obtained by the AERONET sun photometer, as explained in Chazette et al. (2014a) (thus avoiding a bias of up to 10 % above 4 km a.m.s.l., as estimated from our uncorrected signals). We

do not consider temperature dependence of the Raman lines, as the H_2O Raman interference filter is chosen at an insensitive wavelength following Whiteman et al. (2006a). The receiver channels of the lidar were left confined and untouched during the entire campaign to limit variations of the calibration parameters such as was reported by Bock et al. (2014). We trust that this protocol allowed the complete stability found between two calibrations of the WALI, 3 months apart, in its previous involvement (Chazette et al., 2014a).

The overlap function $\xi_{N_2}(z)$ of the N_2 Raman channel is estimated in a homogeneous atmosphere, as provided by a profile with the lidar set up horizontally. In order to assess the missing K_{WVMR} and $\xi_{H_2O}(z)$ in Eq. (1), we performed simultaneous measurements of water vapour by kite ($r_{H_2O,\mathrm{kite}}(z)$) and lidar and computed the following calibration function:

$$C(z) = \frac{S_{H_2O(z)}}{S_{N_2}(z)/\xi_{N_2}(z)} \frac{1}{r_{H_2O,\mathrm{kite}}(z)} \exp(\Delta\tau(z)) \quad (2)$$
$$= \frac{1}{K_{\mathrm{WVMR}}} \xi_{H_2O}(z),$$

the shape of which is that of the overlap factor $\xi_{H_2O}(z)$, and the value at high altitude yields the calibration coefficient K_{WVMR}.

Three flights were performed to assess calibration function $C(z)$, during which the kite remained at a horizontal distance between 60 and 300 m from the laser beam. An important practical constraint was that these flights had to be done in daylight conditions, under which the lidar profiles are affected by sky background noise. Indeed, kite flight is more risky and often restricted in the absence of light. After an initial flight up to 140 m on the afternoon of 22 June, it was determined that the full overlap zone had not been reached. A subsequent flight up to 390 m on the morning of 25 June passed the required altitude to estimate the calibration coefficient. Finally, a third flight was performed during sunset on 25 June when the sky background light was low, to better assess the lowest values of the overlap function, from 0 to 115 m. Note that while this forms the best conditions for lidar calibration, one must anticipate that wind strength can fall quickly at dusk (as experienced on 23 and 24 June). The kite was launched slightly beforehand.

The computed $C(z)$ are given in Fig. 3. The resulting assessment of K_{WVMR} is $94.8 \pm 2.0\,\mathrm{g\,kg^{-1}}$, as a mean over the three flights (note that even if the first flight could not reach the full overlap altitude, as the overlap function remains the same, K_{WVMR} can be evaluated on each flight by dividing $C(z)$ by this function). The uncertainty, estimated between 0.4 and $1.7\,\mathrm{g\,kg^{-1}}$ for each individual flight assuming randomly distributed error with altitude, is predominantly due to lidar noise above 100 m during daytime and to sounding errors at lower altitude or at dusk. Residual standard deviation on the final result will be due to fluctuating bias on either one of the instrument. Full overlap is obtained at 150 m and 50 % overlap is obtained at ~ 90 m; in the following

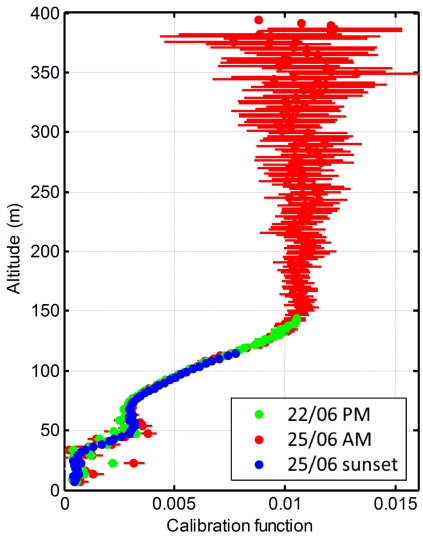

Figure 3. Results of lidar calibration by kite-carried PTU, in terms of calibration function $C(z) = \xi_{H_2O}(z)/K_{\mathrm{WVMR}}$ (dots) as measured during three separate flights: on 22 June afternoon up to 140 m, on 25 June morning up to 390 m and on 25 June at sunset up to 115 m, the latter providing less noisy estimations of the overlap function at low altitude. The RMSE combining lidar signal noise and sounding errors is shown as horizontal bars. The assessed K_{WVMR} is $95 \pm 2\,\mathrm{g\,kg^{-1}}$.

WVMR profile retrievals, we corrected the overlap function down to the latter altitude and discarded the lower profile. We note an unusual shape of the overlap function with a plateau around 50–70 m. Rather than pointing towards a wrong estimation of the N_2 overlap function, verified on five separate occurrences, this effect has already been seen on the elastic channel of other lidars with the same design and has been associated with a bad re-collimation of the received beam on the spectral filtering components. The response of the dichroic beam splitter and interference filter (see Chazette et al., 2014a) to close object points with even more inclined rays is highly variable and may explain this effect. Better focusing of the system on an optical bench should attenuate this phenomenon in future implementations.

4 Validation

In order to validate the kite-calibrated WVMR profile provided by WALI, we first compare it to the radiosoundings carried out at Sant Lluís airfield during the beginning of the ADRIMED campaign (12–17 June 2013), a period characterized by several pollution transport events, followed by a Saharan dust event. We then study the correlation of lidar WVMR profiles with reanalyses of the ECMWF/IFS weather prediction model, over a longer period. Finally, we compare the integrated profile in terms of precipitable water vapour to the retrievals of the AERONET sun photometer,

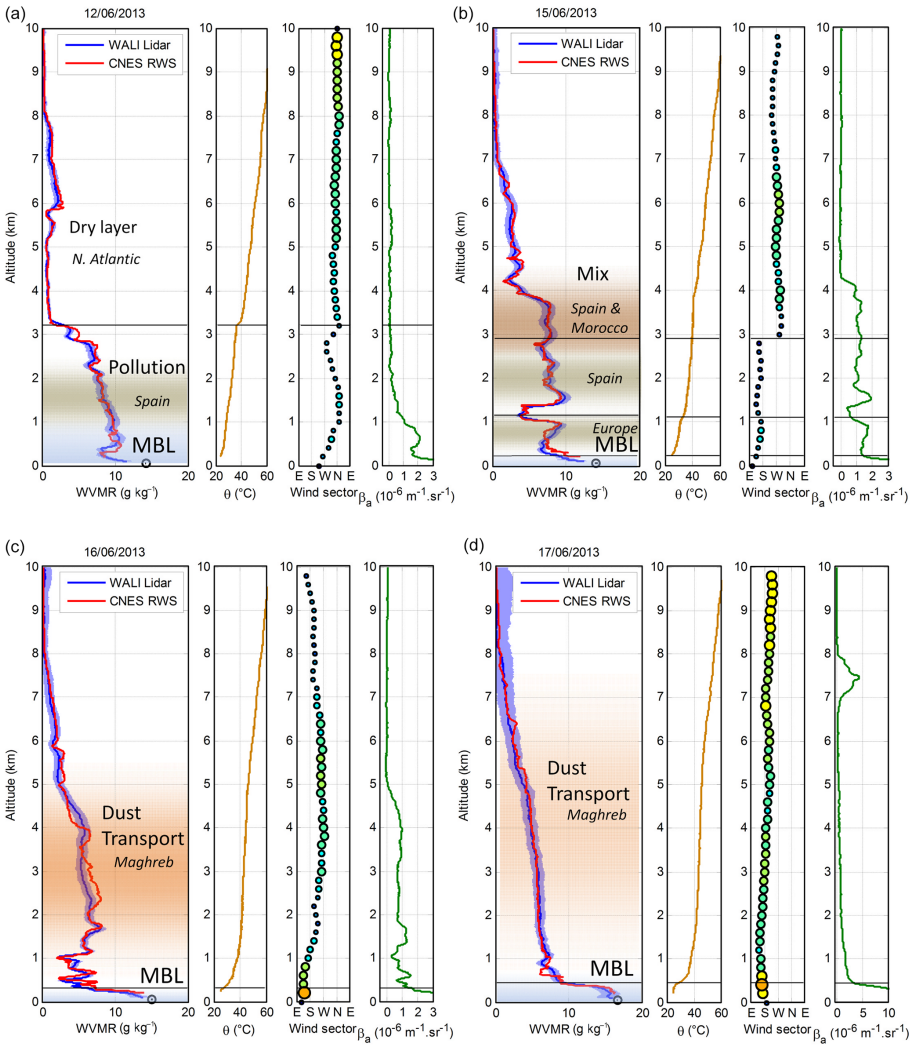

Figure 4. Comparison of lidar WVMR measurements to four rawinsoundings performed from Sant-Lluís air field on the evenings of **(a)** 12 June, **(b)** 15 June, **(c)** 16 June and **(d)** 17 June 2013 (approximately 21:00 to 23:00 LT), under varied aerosol loads and atmospheric water contents. The red line is the radiosonde-derived WVMR and the blue line is that obtained by lidar, with its standard deviation represented as a blue-shaded area. The black circle at zero altitude indicates WVMR as measured on the ground. Potential temperature θ, wind sector and velocity (shown as circle size and colour, measured by the radiosonde), as well as profiles of aerosol backscatter coefficient β_a (measured by the lidar), are also given for reference. Layer boundaries as indicated by wind shears and strong potential temperature gradients are denoted by black lines. Origins and contents of air masses as deduced by back trajectories (HYSPLIT; Draxler and Rolph, 2015) are given in plain text. The lidar integration time is equal to the balloon ascent, i.e. approximately 40 min. MBL stands for marine boundary layer.

the Aqua/MODIS instrument and the ECMWF reanalyses to study the stability of the calibration factor.

4.1 Comparisons to local rawinsoundings

Figure 4 shows the comparison of lidar-derived WVMR to the measurements of balloon radiosondes during their ascent. Note that the lidar integration time is equal to the duration of the ascent phase, approximately 40 min. We recall that the radiosonde uncertainty (not shown for better clarity) is $\sim 1.2\,\mathrm{g\,kg^{-1}}$ at ground level, down to $0.04\,\mathrm{g\,kg^{-1}}$ at 10 km a.m.s.l. The lidar instrumental WVMR uncertainty, calculated from the propagation of short-term profile-to-profile standard deviation as in Chazette et al. (2014a), is shown in blue. For reference, potential temperature, wind sector and velocity given by the sonde and the backscatter coefficient profile given by the lidar are shown. Ground-level WVMR yielded by the Vaisala PTU-300 on a 6 m mast is given by the black circle. Origins and contents of air masses, as deduced from both back trajectories (HYSPLIT; Draxler and Rolph, 2015) and optical parameters retrieved after the

inversion of the other channels of WALI (lidar ratio, particle depolarisation ratio), are given in plain text.

Overall very good agreement is observed in all the comparisons, except at sharp transitions. The altitude of transitions is sometimes shifted and absolute values of WVMR can differ in thin layers. The largest discrepancies occur near the ground, making these non-collocated radiosoundings unsuitable for the measurement of the overlap factor. Moreover, strong deviations are seen in a dust layer on the evening of 16 June. Such an effect remains unexplained, as the most important inhomogeneity, corresponding to a change in circulation, occurred 24 h earlier with little impact.

We assess the calibration factor K_{WVMR} that would have been obtained by using the ratio between radiosounding and lidar, averaged between 1 km and 6 km a.m.s.l. and over all profiles: $K_{\mathrm{WVMR}} = 95.7 \pm 3.5\,\mathrm{g\,kg^{-1}}$. This is compatible with the result of calibration by kite: no drift of the calibration factor is measured during the span of 13 days covered by these comparisons. Note that the above standard deviation, computed using the lidar profile error and the specifications of Table 2, shows a higher value than with the kite, which seems due to the horizontal inhomogeneity of WVMR and maybe also to the shorter averaging time available with balloons quickly ascending through the troposphere.

After the measurements of Fig. 4, average deviations between lidar and radiosondes are plotted in Fig. 5. The mean absolute difference between lidar-derived WVMR versus that of balloon radiosondes is under $\pm 0.2\,\mathrm{g\,kg^{-1}}$ across the whole profile. The root mean square difference (RMSD) is $\sim 1\,\mathrm{g\,kg^{-1}}$ below 1 km a.m.s.l., $< 0.6\,\mathrm{g\,kg^{-1}}$ above 1 km a.m.s.l. and $< 0.2\,\mathrm{g\,kg^{-1}}$ above 7 km a.m.s.l. Not shown but also informative, the mean relative difference (i.e. 2 (lidar−sonde) / (lidar + sonde)) is under ±5 % until 7 km a.m.s.l. Relative RMSD reaches 13 % near the ground, is under 8 % between 1 and 4 km a.m.s.l. and grows to 12 % at 7 km a.m.s.l. At higher altitudes, it diverges up to 40 % at 10 km a.m.s.l. Indeed, depending on SNR the maximum range of the lidar can be reached between 7.5 and 10 km a.m.s.l., above which the retrieved WVMR is null per our processing algorithm (truncation at SNR = 5 on the N_2 Raman channel).

Note that the balloons have already travelled between 15 and 20 km from the lidar when at 7 km a.m.s.l. Recently, the fine-scale horizontal structure function of WVMR in the free troposphere was assessed using a DIAL lidar onboard an airplane travelling across several hundred kilometres (Fischer et al., 2013). By taking – from Fig. 2 of the cited reference – the order 2 structure function estimated at 4.1 km a.m.s.l. in a non-convective case, one can straightforwardly estimate the RMSD of WVMR between two points horizontally separated by distance d to scale as $\Delta r_{\mathrm{H_2O,RMS}}(d)/\langle r_{\mathrm{H_2O}}\rangle \approx 14\,\%\,(d/10\,\mathrm{km})^{0.6}$. This amounts to $\sim 19\,\%$ for the balloon drift of 20 km given above and would explain a majority of the observed RMSD between lidar and balloons around this altitude.

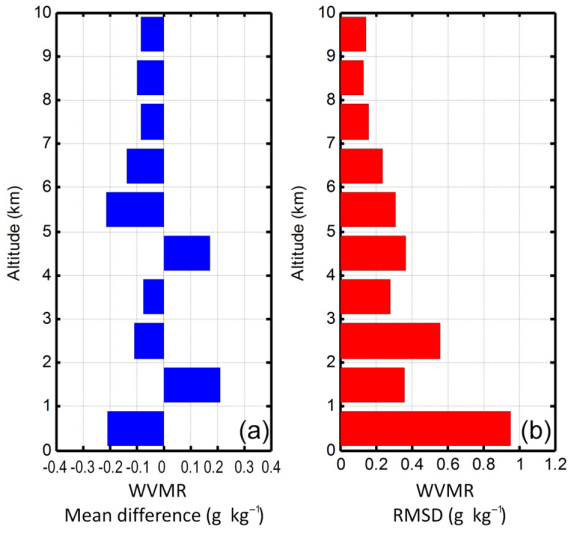

Figure 5. Average deviations between profiles of WVMR by balloon radiosondes and lidar shown in Fig. 4: **(a)** mean difference and **(b)** root mean square difference (RMSD).

4.2 Long-term correlation with NWP model reanalyses

In order to extend this validation to a broader data set, we compare a longer period of lidar measurements (12–28 June) to the ECMWF/IFS reanalyses over Menorca, resulting in the scatter plot shown in Fig. 6a. We also plot root mean square difference ($\mathrm{RMSD}(x,y) = \langle (x-y)^2\rangle^{1/2}$) and correlation coefficient ($\mathrm{COR}(x,y) = \langle (x-\langle x\rangle)(y-\langle y\rangle)\rangle/(\mathrm{var}(x)\mathrm{var}(y))^{1/2}$) between the two profiles as defined in Boylan and Russell (2006). The scatter plot demonstrates very little bias in terms of lidar calibration, except for the lower values ($< 2\,\mathrm{g\,kg^{-1}}$) which are mostly found in the upper layers that can be out of range of the lidar. There is however some dispersion around the identity line, investigated against altitude in terms of RMSD and COR in Fig. 6b and c. We see that the higher RMSDs ($\sim 1.5\,\mathrm{g\,kg^{-1}}$) between lidar and model occur mostly in the lower troposphere (below 3 km), where moisture may vary rapidly and might not be well resolved by the model. Between 3 and 5 km a.m.s.l., a correlation coefficient around 0.9 is found, which is satisfactory.

For completeness, we also compared the lidar profiles to the operational meteorology radiosoundings performed twice daily at Palma de Majorca (39°34′ N, 2°39′ E; 135 km ESE of Cap d'en Font). The results are not shown here because the observed moderate value of correlation (~ 0.6–0.7) in the middle free troposphere, and even worse in the boundary layer, was mostly due to the long baseline between the lidar and Palma. The NWP model reanalyses remain necessary to interpolate the radiosounding data at the location of the lidar.

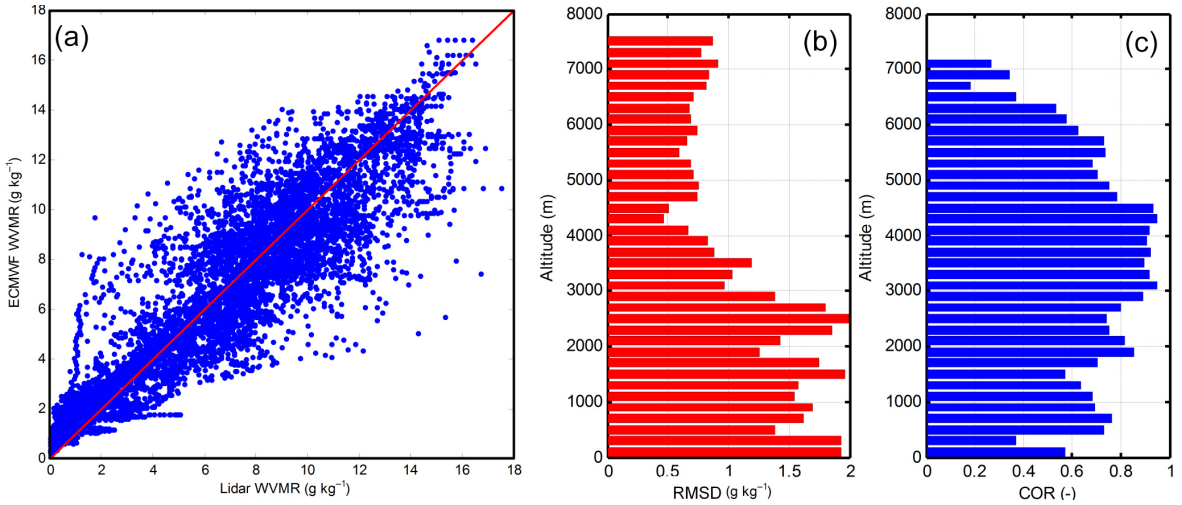

Figure 6. (a) Scatter plot between ECMWF and lidar-derived WVMR over all simultaneous measurements (blue dots). The red line is the identity. **(b)** Root mean square difference and **(c)** correlation between simultaneous profiles as a function of altitude (RMSD and COR as defined in the text).

In conclusion, we see that WVMR profiles obtained by lidar are well correlated with model reanalyses (which interpolate all moisture measurements in the area), further validating WALI and its calibration over a long period. There is however an impact of strong WVMR inhomogeneity in the lower layers including the marine boundary layer (< 500 m a.m.s.l.), which are not resolved by the model.

4.3 Intercomparisons of integrated water content

Thanks to the ability of the calibrated lidar to measure the bottommost layers (down to 90 m), another quantitative comparison can be made by integrating the night-time WVMR lidar profile over the whole atmospheric column to obtain precipitable water vapour content (PWV) $\mathrm{WV_p}$ as

$$\mathrm{WV_p} = \int_{z=0}^{z=z_{\max}} \frac{\rho_{\mathrm{air,dry}}(z)}{\rho_{\mathrm{water}}} r_{\mathrm{H_2O}}(z)\mathrm{d}z, \quad (3)$$

where $z_{\max}$ is the maximum altitude of the night-time lidar measurements ($z_{\max} = 10$ km a.m.s.l.), $\rho_{\mathrm{air,dry}}(z)$ the density profile of dry air, which is here deduced from the ECMWF model, and $\rho_{\mathrm{water}} = 10^3\,\mathrm{kg\,m^{-3}}$ the density of water. Note that the lidar WVMR profiles have been prolonged down to the ground by linearly interpolating between the value at 90 m above ground level (a.g.l.) and the measurement of the Vaisala PTU-300 on a 6 m a.g.l. mast at the lidar station.

Lidar PWV can be compared directly to that derived from the WVMR profiles obtained by radiosounding at Sant Lluís and by the ECMWF model as well as to products given by AERONET and MODIS on Terra and Aqua (discarding cloudy pixels with lesser PWV). The aim of this section is not to intercompare water vapour measurement techniques, which has been done extensively elsewhere (e.g. Bock et al., 2013), but to further validate the accuracy of the lidar and especially the stability of the calibration factor, shown to vary by 17 % over 45 days in the same study by Bock et al. (2013).

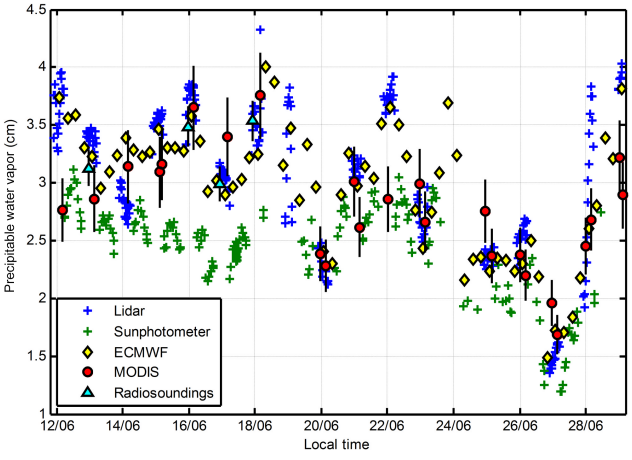

Figure 7. Comparison of various retrievals of integrated water vapour content (precipitable water vapour, PWV, in cm) from 12 to 19 June 2013: by lidar (blue), AERONET sun photometer (green), MODIS (average within a 10 km radius area around the lidar, discarding cloudy pixels with lower PWV, red circles), ECMWF 0.5° model reanalyses (interpolation, yellow diamonds) and radiosoundings at Menorca (cyan triangles, error bars computed after uncertainty in Table 1) as a reference. Error bars given for MODIS represent 10 % relative error (Pérez-Ramirez et al., 2014).

PWV retrievals are plotted as a function of time for 12–29 June period in Fig. 7. The AERONET sun-photometer-derived PWV and, to a lower extent, the MODIS PWV level 2 product show the most discrepancies with other measurements.

Table 2. Statistics for the comparison between various integrated water vapour content retrievals and the lidar (simultaneous measurements within ±1 h).

	Mean bias (cm)	SD (cm)	Mean rel. bias (%)	Rel. SD (%)
Sun photometer	−0.93	0.92	−28	28
ECMWF	−0.08	0.26	−1.5	8.9
ECMWF (w/o 6/14)	−0.12	0.18	−2.7	5.8
MODIS	−0.17	0.50	−3.1	15.6
Radiosoundings	−0.15	0.19	−4.0	6

The sun photometer PWV did not pass 3 cm for the whole period, generating a strong mean negative bias of −0.93 cm compared to the lidar. The strong diurnal variation on sun-photometer-derived PWV observed in the figure seems to be correlated with the diurnal evolution of the solar zenith angle. While several studies have commended the reliability of the AERONET retrieval, compared to GPS for instance (Bock et al., 2013), others warn about a slight dry bias (Pérez-Ramirez et al., 2014) and the impact of misty and slightly cloudy weather (Liu et al., 2013) or of an improper calibration of the sun photometer (Schmid et al., 2001). However, the lidar observations ensure that sun photometer measurements were acquired under perfectly cloud-free conditions, the sun photometer was recently calibrated, and the AERONET retrieval at Palma (not shown here) was similarly very strongly biased. This excludes both weather- or instrument-related problems and points towards a systematic error of the retrieval method or calibration process.

For MODIS, the PWV uncertainty is estimated to lie between 5 and 10 % (Gao and Kaufman, 2003), which explains part of the discrepancies observed (about 15 % standard deviation overall). On 12, 22 and 29 June, however, the MODIS retrieval is significantly lower than that of the lidar and the ECMWF reanalyses. A possible explanation is that cirrus contamination is suspected over the whole area on these days, which would have biased MODIS PWV (given "above the cloud level") towards lower values.

In contrast, both ECMWF and radiosonde retrievals lie much closer to the lidar values (5.5 and 4.5 % RMSD respectively), validating the soundness of absolute lidar-derived PWV. The largest difference is seen on 14 June, when a very dry layer is seen extending down to 2 km a.m.s.l. by the lidar, whereas the ECMWF/IFS model does not see it as low. This can explain the larger PWV found by the model. Excluding this particular measurement, the relative mean (resp. standard) deviation between lidar and other retrievals is only −1 % (resp. 11 % RMSD). If we further restrain the comparison to the most reliable data given by radiosoundings and ECMWF/IFS, RMSD is less than 6 %. Above these random errors, no consistent drift is found for the calibration factor of the lidar over the 17 days of this study, in contrast to other instruments. If there is a drift, it must be much smaller than 10 %. This good stability may be due to the careful confinement of the lidar in its carrier van, equipped with powerful air conditioning.

5 Summary and conclusions

The aerosol/H_2O/N_2 Raman lidar WALI was implemented in response to the main scientific questions of the HyMeX research project about the water cycle over the western Mediterranean basin. In the framework of the ChArMEx/ADRIMED special observation period, WALI was deployed on Menorca from June to July 2013 for complementary studies on tropospheric water vapour content and aerosols. During each field experiment, the WVMR profiles derived from WALI measurements have to be calibrated locally for maximum accuracy and to retrieve the overlap factor of the lidar. Radiosounding measurements from the approved balloon launch site were prone to sample a different air mass, which could be aggravated by balloon drifting. In our case, due to the separation between the launch site and the lidar station, the RMSD could reach $\sim 1\,\mathrm{g\,kg^{-1}}$ in the first kilometres of the troposphere.

We used a meteorological probe lifted by a kite launched from the lidar site, allowing a relative uncertainty of 2 % on WVMR calibration, down to 90 m a.g.l., thanks to the co-located measurement and the slower ascent permitted by the kite. After several trials, a ∼ 45 min flight up to 300 m at dusk (for better lidar SNR) seems to be optimal for this method. The calibration uncertainty achieved with this method is better than the one reached for the previous deployment of WALI (with radiosoundings and a plane-carried sonde; Chazette et al., 2014a). It is predominantly due to lidar noise above 100 m during daytime and to uncertainty on the kite measurements at lower altitude or at dusk. The relative calibration uncertainty is in the same range as the one of 1.4 % obtained with microwave radiometers over long periods by Foth et al. (2015) and better than the 4.5 % reached with several night-time radiosoundings by Whiteman et al. (2006a) and confirmed here. We find that the kite-borne method has suitable precision and allows characterising the lidar overlap function, while being lighter to implement.

The calibrated WVMR profiles have been cross-compared with radiosoundings, as well as integrated moisture derived from satellite measurements and the ECMWF/IFS reanaly-

ses. The profiles are shown to be in very good agreement in the free troposphere (1–5 km a.m.s.l., mean absolute deviations within 0.2 g kg^{-1}, ±5 % relative), less so in the marine boundary layer due to inhomogeneity, and above 7–8 km a.m.s.l. due to the range limitation of the lidar. Deviations between integrated water vapour contents appear to be within 6 % RMSE (compared to model reanalyses and local radiosoundings), and no drift is reported over the measurement period of ∼ 3 weeks. The MODIS level 2 data of PWV do not agree as well, with a RMSD ∼ 15 % comparatively with the PWV derived from WALI. Finally, large discrepancies (more than −1 cm bias) are observed when considering the sun-photometer-derived PWV. The fact that sun photometer measurements were acquired in verifiably cloud-free conditions, that the sun photometer was recently calibrated, and that the AERONET retrievals at Palma were similarly very strongly biased excludes both weather- or instrument-related problems and points towards a systematic error of the retrieval method or calibration process. It may still be specific to the conditions experienced in the Balearic sea during this period. While several previous studies have warned about a slight dry bias (Pérez-Ramirez et al., 2014) or wet/dry biases and drifts below 0.3 cm depending on the Cimel sun photometer used (Torres et al., 2009), this much stronger effect (up to 1 cm) has not been reported elsewhere, to our knowledge, despite multiple works on the subject (Estellés et al., 2007; Martinez-Lozano et al., 2007; Mavromatakis et al., 2007; Ortiz de Galisteo et al., 2010). It should be investigated further, by comparison to GPS network retrievals for instance, in similar conditions. However, overall the lidar calibration is found to be accurate and stable over the period.

Assuming full lidar overlap at the maximum sounding altitude and no bias at higher altitude, kite sounding therefore appears to be a practical and reliable way to calibrate both the water vapour retrieval and overlap factor of a H_2O Raman lidar, thanks to maximum SNR, longer sounding and immediate proximity to the lidar beam. Limitations include the need for good wind conditions, although only a couple of knots are enough and frequent in many open sites, and regulations due to air traffic control, which vary geographically. This technique could be extended to any physical parameter measurable both by a lidar and a probe weighting less than a kilogram, such as temperature, aerosol size distribution, concentration or optical properties.

This calibration method may be considered within the context of medium-term prospects such as the operational use of H_2O Raman lidar systems for monitoring water vapour content in the low and middle troposphere. Such monitoring will provide the necessary constraints to forecast extreme precipitation events, like those encountered during autumn 2015 on the orography of the western Mediterranean basin. Indeed, during the upstream phase of HyMeX, a good coherence was found between the water vapour mixing ratio profiles measured by WALI and those estimated by mesoscale model reanalyses of AROME-WMED and ECMWF/IFS (Chazette et al., 2015a, b).

Acknowledgements. The authors thank P. Fabre for providing the kites, as well as S. Hassanzadeh, S. Bertolin and M. Jeannot for their precious help during the kite sounding. The lidar station at Menorca was set up and maintained with the help of F. Dulac, F. Marnas and X. Shang from LSCE and M. Sicard, C. Munoz and D. Lange from Universitat de Catanlunya. Balloon radiosoundings were performed by N. Verdier from CNES. AERONET, NASA (MODIS) and ECMWF are acknowledged for graciously making their data sets available for this work. We finally thank Z. Harris for her precious help in correcting the manuscript. This work was funded by the HyMeX and ChArMEx components of the MISTRALS program, the MUSIC grant ANR-14–CE01-01 and by the Commissariat à l'Energie Atomique.

Edited by: O. Dubovik

References

Behrendt, A., Wulfmeyer, V., Riede, A., Wagner, G., Pal, S., Bauer, H., Radlach, M., and Späth, F.: 3-Dimensional observations of atmospheric humidity with a scanning differential absorption lidar, in: Proc. SPIE Vol. 7475, Remote Sensing of Clouds and the Atmosphere XIV, edited by R. H. Picard, K. Schäfer, A. Comeron, and M. van Weele, 74750L, doi:10.1117/12.835143, 2009.

Bhawar, R., Di Girolamo, P., Summa, D., Flamant, C., Althausen, D., Behrendt, A., Kiemle, C., Bosser, P., Cacciani, M., Champollion, C., Di Iorio, T., Engelmann, R., Herold, C., Müller, D., Pal, S., Wirth, M., and Wulfmeyer, V.: The water vapour intercomparison effort in the framework of the convective and orographically-induced precipitation study: airborne-to-ground-based and airborne-to-airborne lidar systems, Q. J. Roy. Meteor. Soc., 137, 345–348, doi:10.1002/qj.697, 2011.

Bock, O., Bosser, P., Bourcy, T., David, L., Goutail, F., Hoareau, C., Keckhut, P., Legain, D., Pazmino, A., Pelon, J., Pipis, K., Poujol, G., Sarkissian, A., Thom, C., Tournois, G., and Tzanos, D.: Accuracy assessment of water vapour measurements from in situ and remote sensing techniques during the DEMEVAP 2011 campaign at OHP, Atmos. Meas. Tech., 6, 2777–2802, doi:10.5194/amt-6-2777-2013, 2013.

Boylan, J. W. and Russell, A. G.: PM and light extinction model performance metrics, goals, and criteria for three-dimensional air quality models, Atmos. Environ., 40, 4946–4959, doi:10.1016/j.atmosenv.2005.09.087, 2006.

Chazette, P., Marnas, F., and Totems, J.: The mobile Water vapor Aerosol Raman LIdar and its implication in the framework of the HyMeX and ChArMEx programs: application to a dust transport process, Atmos. Meas. Tech., 7, 1629–1647, doi:10.5194/amt-7-1629-2014, 2014a.

Chazette, P., Marnas, F., Totems, J., and Shang, X.: Comparison of IASI water vapor retrieval with H_2O-Raman lidar in the framework of the Mediterranean HyMeX and ChArMEx programs, Atmos. Chem. Phys., 14, 9583–9596, doi:10.5194/acp-14-9583-2014, 2014b.

Chazette, P., Flamant, C., Raut, J.-C., Totems, J., and Shang, X.: Tropical moisture enriched storm tracks over the Mediterranean

and their link with intense rainfall in the Cevennes-Vivarais area during HyMeX, Q. J. Roz. Meteor. Soc., doi:10.1002/qj.2674, online first, 2015a.

Chazette, P., Flamant, C., Shang, X., Totems, J., Raut, J.-C., Doerenbecher, A., Ducrocq, V., Fourrié, N., Bock, O. and Cloché, S.: A multi-instrument and multi-model assessment of atmospheric moisture variability over the Western Mediterranean during HyMeX, Q. J. Roz. Meteor. Soc., doi:10.1002/qj.2671, online first, 2015b.

Davidson, K. L., Guest, P. S., Mabey, D. L., Frederickson, P. A., Anderson, K. D., Doss-Hammel, S. M., and Tsintikidis, D.: The use of kite observations to study air–sea interaction-controlled atmospheric surface layer profiles during the RED experiment, in: 12th Conference on Interactions of the Sea and Atmosphere, vol. 1, available at: http://calhoun.nps.edu/public/handle/10945/41312 (last access: 19 September 2014), 2003.

Di Girolamo, P., Summa, D., Lin, R.-F., Maestri, T., Rizzi, R., and Masiello, G.: UV Raman lidar measurements of relative humidity for the characterization of cirrus cloud microphysical properties, Atmos. Chem. Phys., 9, 8799–8811, doi:10.5194/acp-9-8799-2009, 2009.

Dionisi, D., Keckhut, P., Courcoux, Y., Hauchecorne, A., Porteneuve, J., Baray, J. L., Leclair de Bellevue, J., Vérèmes, H., Gabarrot, F., Payen, G., Decoupes, R., and Cammas, J. P.: Water vapor observations up to the lower stratosphere through the Raman lidar during the Maïdo Lidar Calibration Campaign, Atmos. Meas. Tech., 8, 1425–1445, doi:10.5194/amt-8-1425-2015, 2015.

Draxler, R. R. and Rolph, G. D.: HYSPLIT (HYbrid Single-Particle Lagrangian Integrated Trajectory) Model access via NOAA ARL READY Website, NOAA Air Resour. Lab. Silver Spring, MD, available at: http://ready.arl.noaa.gov/HYSPLIT.php, last access: 20 August, 2015.

Drobinski, P., Ducrocq, V., Alpert, P., Anagnostou, E., Béranger, K., Borga, M., Braud, I., Chanzy, A., Davolio, S., Delrieu, G., Estournel, C., Boubrahmi, N. F., Font, J., Grubišić, V., Gualdi, S., Homar, V., Ivančan-Picek, B., Kottmeier, C., Kotroni, V., Lagouvardos, K., Lionello, P., Llasat, M. C., Ludwig, W., Lutoff, C., Mariotti, A., Richard, E., Romero, R., Rotunno, R., Roussot, O., Ruin, I., Somot, S., Taupier-Letage, I., Tintore, J., Uijlenhoet, R., and Wernli, H.: HyMeX: A 10-year multidisciplinary program on the mediterranean water cycle, B. Am. Meteorol. Soc., 95, 1063–1082, doi:10.1175/BAMS-D-12-00242.1, 2014.

Ducrocq, V., Braud, I., Davolio, S., Ferretti, R., Flamant, C., Jansa, A., Kalthoff, N., Richard, E., Taupier-Letage, I., Ayral, P.-A., Belamari, S., Berne, A., Borga, M., Boudevillain, B., Bock, O., Boichard, J.-L., Bouin, M.-N., Bousquet, O., Bouvier, C., Chiggiato, J., Cimini, D., Corsmeier, U., Coppola, L., Cocquerez, P., Defer, E., Delanoë, J., Di Girolamo, P., Doerenbecher, A., Drobinski, P., Dufournet, Y., Fourrié, N., Gourley, J. J., Labatut, L., Lambert, D., Le Coz, J., Marzano, F. S., Molinié, G., Montani, A., Nord, G., Nuret, M., Ramage, K., Risøn, W., Roussot, O., Said, F., Schwarzenboeck, A., Testor, P., Van Baelen, J., Vincendon, B., Aran, M., and Tamayo, J.: HyMeX-SOP1: the field campaign dedicated to heavy precipitation and flash flooding in the northwestern Mediterranean, B. Am. Meteorol. Soc., 95, 1083–1100, doi:10.1175/BAMS-D-12-00244.1, 2014.

Estellés, V., Martínez-Lozano, J. A., Utrillas, M. P., and Campanelli, M.: Columnar aerosol properties in Valencia (Spain) by ground-based Sun photometry, J. Geophys. Res., 112, D11201, doi:10.1029/2006JD008167, 2007.

Fischer, L., Craig, G. C., and Kiemle, C.: Horizontal structure function and vertical correlation analysis of mesoscale water vapour variability observed by airborne lidar, J. Geophys. Res. Atmos., 118, 7579–7590, doi:10.1002/jgrd.50588, 2013.

Foth, A., Baars, H., Di Girolamo, P., and Pospichal, B.: Water vapour profiles from Raman lidar automatically calibrated by microwave radiometer data during HOPE, Atmos. Chem. Phys., 15, 7753–7763, doi:10.5194/acp-15-7753-2015, 2015.

Gao, B.-C. and Kaufman, Y. J.: Water vapour retrievals using Moderate Resolution Imaging Spectroradiometer (MODIS) near-infrared channels, J. Geophys. Res., 108, 4389, doi:10.1029/2002JD003023, 2003.

Haywood, J. M., Roberts, D. L., Slingo, A., Edwards, J. M., and Shine, K. P.: General Circulation Model Calculations of the Direct Radiative Forcing by Anthropogenic Sulfate and Fossil-Fuel Soot Aerosol, J. Climate, 10, 1562–1577, doi:10.1175/1520-0442(1997)010<1562:GCMCOT>2.0.CO;2, 1997.

IPCC: Climate Change 2014: Impacts, Adaptation, and Vulnerability. Part A: Global and Sectoral Aspects, Contribution of Working Group II to the Fifth Assessment Report of the Intergovernmental Panel on Climate Change, edited by: C. B. Field, V. R. Barros, D. J. Dokken, K. J. Mach, M. D. Mastrandrea, T. E. Bili, M. Chatterjee, K. L. Ebi, Y. O. Estrada, R. C. Genova, B. Girma, E. S. Kissel, A. N. Levy, S. MacCracken, P. R. Mastrandrea, and L. L. White, Cambridge University Press, Cambridge, UK and New York, NY, USA, 2014.

Kulmala, M.: Condensational Growth and Evaporation in the Transition Regime, Aerosol Sci. Technol., 19, 381–388, doi:10.1080/02786829308959645, 1993.

Leblanc, T. and McDermid, I. S.: Accuracy of Raman lidar water vapour calibration and its applicability to long-term measurements., Appl. Optics, 47, 5592–603, 2008.

Liu, Z., Li, M., Zhong, W., and Wong, M. S.: An approach to evaluate the absolute accuracy of WVR water vapour measurements inferred from multiple water vapour techniques, J. Geodyn., 72, 86–94, doi:10.1016/j.jog.2013.09.002, 2013.

Mallet, M., Dulac, F., Formenti, P., Nabat, P., Sciare, J., Roberts, G., Pelon, J., Ancellet, G., Tanré, D., Parol, F., Denjean, C., Brogniez, G., di Sarra, A., Alados-Arboledas, L., Arndt, J., Auriol, F., Blarel, L., Bourrianne, T., Chazette, P., Chevaillier, S., Claeys, M., D'Anna, B., Derimian, Y., Desboeufs, K., Di Iorio, T., Doussin, J.-F., Durand, P., Féron, A., Freney, E., Gaimoz, C., Goloub, P., Gómez-Amo, J. L., Granados-Muñoz, M. J., Grand, N., Hamonou, E., Jankowiak, I., Jeannot, M., Léon, J.-F., Maillé, M., Mailler, S., Meloni, D., Menut, L., Momboisse, G., Nicolas, J., Podvin, T., Pont, V., Rea, G., Renard, J.-B., Roblou, L., Schepanski, K., Schwarzenboeck, A., Sellegri, K., Sicard, M., Solmon, F., Somot, S., Torres, B, Totems, J., Triquet, S., Verdier, N., Verwaerde, C., Waquet, F., Wenger, J., and Zapf, P.: Overview of the Chemistry-Aerosol Mediterranean Experiment/Aerosol Direct Radiative Forcing on the Mediterranean Climate (ChArMEx/ADRIMED) summer 2013 campaign, Atmos. Chem. Phys., 16, 455–504, doi:10.5194/acp-16-455-2016, 2016.

Martinez-Lozano, J. A., Estelles, V., Molero, F., Gomez-Amo, J. L., Utrillas, M. P., Pujadas, M., Fortea, J. C., and Guanter, L.: Atmospheric Components Determination From Ground-Level Measurements During the Spectra Barax Campaigns (SPARC) Field Campaigns, IEEE Trans. Geosci. Remote Sens., 45, 2778–2793, doi:10.1109/TGRS.2007.902295, 2007.

Mavromatakis, F., Gueymard, C. A., and Franghiadakis, Y.: Technical Note: Improved total atmospheric water vapour amount determination from near-infrared filter measurements with sun photometers, Atmos. Chem. Phys., 7, 4613–4623, doi:10.5194/acp-7-4613-2007, 2007.

Melfi, S. H., Whiteman, D., and Ferrare, R.: Observation of Atmospheric Fronts Using Raman Lidar Moisture Measurements, J. Appl. Meteorol., 28, 789–806, doi:10.1175/1520-0450(1989)028<0789:OOAFUR>2.0.CO;2, 1989.

Ortiz de Galisteo, J. P., Toledano, C., Cachorro, V., and Torres, B.: Improvement in PWV estimation from GPS due to the absolute calibration of antenna phase center variations, GPS Solut., 14, 389–395, doi:10.1007/s10291-010-0163-y, 2010.

Pérez-Ramirez, D., Whiteman, D. N., Smirnov, A., Lyamani, H., Holben, B. N., Pinker, R., Andrade, M., and Alados-Arboledas, L.: Evaluation of AERONET precipitable water vapour vs. micro-wave radiometry, GPS, and radiosondes at ARM sites, J. Geophys. Res. Atmos., 119, 9596–9613, doi:10.1002/2014JD021730, 2014.

Randriamiarisoa, H., Chazette, P., Couvert, P., Sanak, J., and Mégie, G.: Relative humidity impact on aerosol parameters in a Paris suburban area, Atmos. Chem. Phys., 6, 1389–1407, doi:10.5194/acp-6-1389-2006, 2006.

Reiche, M., Funk, R., Zhang, Z., and Hoffmann, C.: Using a parafoil kite for measurement of variations in particulate matter – a kite-based dust profiling approach, Atmos. Clim. Sci., 2, 41–51, doi:10.4236/acs.2012.21006, 2012.

Rood, M. J., Covert, D. S., and Larson, T. V.: Hygroscopic properties of atmospheric aerosol in Riverside, California, Tellus B, 39, 383–397, doi:10.1111/j.1600-0889.1987.tb00201.x, 1987.

Schmid, B., Michalsky, J. J., Slater, D. W., Barnard, J. C., Halthore, R. N., Liljegren, J. C., Holben, B. N., Eck, T. F., Livingston, J. M., Russell, P. B., Ingold, T., and Slutsker, I.: Comparison of columnar water-vapour measurements from solar transmittance methods, Appl. Optics, 40, 1886, doi:10.1364/AO.40.001886, 2001.

Sherlock, V., Garnier, A., Hauchecorne, A., and Keckhut, P.: Implementation and validation of a Raman lidar measurement of middle and upper tropospheric water vapour, Appl. Optics, 38, 5838, doi:10.1364/AO.38.005838, 1999a.

Sherlock, V., Hauchecorne, A., and Lenoble, J.: Methodology for the independent calibration of Raman backscatter water-vapour lidar systems., Appl. Optics, 38, 5816–37, doi:10.1364/AO.38.005838, 1999b.

Torres, B., Cachorro, V. E., Toledano, C., Ortiz de Galisteo, J. P., Berjón, A., de Frutos, A. M., Bennouna, Y., and Laulainen, N.: Precipitable water vapor characterization in the Gulf of Cadiz region (southwestern Spain) based on Sun photometer, GPS, and radiosonde data, J. Geophys. Res., 115, D18103, doi:10.1029/2009JD012724, 2009.

Turner, D. D., Whiteman, D. N., Evans, K. D., Melfi, S. H., Goldsmith, J. E. M., and Schwemmer, G. K.: Water vapour measurements by Raman lidar during the ARM 1997 Water Vapour Intensive Observation Period, in: IGARSS'98. Sensing and Managing the Environment, 1998 IEEE International Geoscience and Remote Sensing, Symposium Proceedings, vol. 4, 2155–2157, 1998.

Weckwerth, T. M., Wulfmeyer, V., Wakimoto, R. M., Hardesty, R. M., Wilson, J. W., and Banta, R. M.: NCAR–NOAA lower-tropospheric water vapour workshop, B. Am. Meteorol. Soc., 80, 2339–2357, doi:10.1175/1520-0477(1999)080<2339:NNLTWV>2.0.CO;2, 1999.

Weckwerth, T. M., Parsons, D. B., Koch, S. E., Moore, J. a., LeMone, M. a., Demoz, B. B., Flamant, C., Geerts, B., Wang, J., and Feltz, W. F.: An overview of the international H_2O project (IHOP_2002) and some preliminary highlights, B. Am. Meteorol. Soc., 85, 253–277, doi:10.1175/BAMS-85-2-253, 2004.

Whiteman, D. N., Melfi, S., and Ferrare, R.: Raman lidar system for the measurement of water vapour and aerosols in the Earth's atmosphere, Appl. Optics, 31, 3068–82, doi:10.1364/AO.31.003068, 1992.

Whiteman, D. N., Demoz, B., Schwemmer, G., Gentry, B., Di Girolamo, P., Sabatino, D., Comer, J., Veselovskii, I., Evans, K., Lin, R.-F., Wang, Z., Behrendt, A., Wulfmeyer, V., Browell, E., Ferrare, R., Ismail, S., and Wang, J.: Raman lidar measurements during the international H_2O project. Part I: Instrumentation and analysis techniques, J. Atmos. Ocean. Tech., 23, 157–169, doi:10.1175/JTECH1839.1, 2006a.

Whiteman, D. N., Demoz, B., Schwemmer, G., Gentry, B., Di Girolamo, P., Sabatino, D., Comer, J., Veselovskii, I., Evans, K., Lin, R.-F., Wang, Z., Behrendt, A., Wulfmeyer, V., Browell, E., Ferrare, R., Ismail, S., and Wang, J.: Raman lidar measurements during the international H_2O project. Part II: Case studies, J. Atmos. Ocean. Tech., 23, 170–183, doi:10.1175/JTECH1839.1, 2006b.

Whiteman, D. N., Venable, D., and Landulfo, E.: Comments on "Accuracy of Raman lidar water vapour calibration and its applicability to long-term measurements," Appl. Optics, 50, 2170–2176 (author reply 2177–2178), doi:10.1364/AO.50.002170, 2011.

Willitsford, A. and Philbrick, C. R.: Lidar description of the evapourative duct in ocean environments, in: Proc. SPIE Vol. 5885, Remote Sensing of the Coastal Oceanic Environment, edited by: R. J. Frouin, M. Babin, and S. Sathyendranath, 58850G, doi:10.1117/12.620948, 2005.

Wulfmeyer, V., Behrendt, A., Kottmeier, C., Corsmeier, U., Barthlott, C., Craig, G. C., Hagen, M., Althausen, D., Aoshima, F., Arpagaus, M., Bauer, H.-S., Bennett, L., Blyth, A., Brandau, C., Champollion, C., Crewell, S., Dick, G., Di Girolamo, P., Dorninger, M., Dufournet, Y., Eigenmann, R., Engelmann, R., Flamant, C., Foken, T., Gorgas, T., Grzeschik, M., Handwerker, J., Hauck, C., Höller, H., Junkermann, W., Kalthoff, N., Kiemle, C., Klink, S., König, M., Krauss, L., Long, C. N., Madonna, F., Mobbs, S., Neininger, B., Pal, S., Peters, G., Pigeon, G., Richard, E., Rotach, M. W., Russchenberg, H., Schwitalla, T., Smith, V., Steinacker, R., Trentmann, J., Turner, D. D., van Baelen, J., Vogt, S., Volkert, H., Weckwerth, T., Wernli, H., Wieser, A., and Wirth, M.: The convective and orographically-induced precipitation study (COPS): the scientific strategy, the field phase, and research highlights, Q. J. Roy. Meteor. Soc., 137, 3–30, doi:10.1002/qj.752, 2011.